Journal of Molecular and Cellular Cardiology Plus 1 (2022) 100011

Contents lists available at ScienceDirect

Journal of Molecular and Cellular Cardiology Plus

journal homepage: https://www.journals.elsevier.com/journal-of-molecular-and-cellular-cardiology-plus

Multiomic analyses reveal enriched glycolytic processes in β-myosin heavy chain-expressed cardiomyocytes in early cardiac hypertrophy

Hsiao-hui Yeh [a,b], Yao-Ming Chang [a], Yu-Wang Chang [a], Mei-Yeh Jade Lu [c], Yi-Hua Chen [c], Chia-Che Lee [c], Chien-Chang Chen [a,b,*]

[a] Institute of Biomedical Sciences, Academia Sinica, Taipei, Taiwan
[b] Taiwan International Graduate Program in Molecular Medicine, National Yang Ming Chiao Tung University and Academia Sinica, Taipei, Taiwan
[c] Biodiversity Research Center, Academia Sinica, Taipei, Taiwan

ARTICLE INFO

Keywords:
Cardiomyocytes
Hypertrophy
Fetal genes
Glycolysis
Transcriptome
Proteome
Spatial transcriptome

ABSTRACT

Background: Cardiac pressure overload induces cardiac hypertrophy and eventually leads to heart failure. One distinct feature of pathological cardiac hypertrophy is fetal-gene re-expression, but not every cardiomyocyte exhibits fetal gene re-expression in the diseased heart. Adult cardiomyocytes are terminally differentiated cells, so we do not know how the heterogeneity is determined and whether the differential fetal-gene reprogramming indicates a different degree of remodeling among cardiomyocytes. We hypothesized that fetal gene-expressed cardiomyocytes show more pathological features in the pressure-overloaded heart.

Results: We induced pressure overload in mice by transverse aortic constriction (TAC) and observed a cardiomyocyte population with expression of β-myosin heavy chain (βMHC, a fetal gene encoded by *Myh7*) after TAC for 3 days. On transcriptomic and proteomic analyses, βMHC-expressed cardiomyocytes of 3-day TAC hearts were enriched in genes in cardiomyopathy-associated pathways and glycolytic processes. Moreover, results of immunoblotting and enzyme activity assay suggested higher glycolytic activity in βMHC-expressed than non-expressed cardiomyocytes. When we inhibited the glycolytic flux by 2-deoxy-D-glucose, a widely used glycolysis inhibitor, the number of βMHC-expressed cardiomyocytes was reduced, and the level of TEA domain family member 1 (TEAD1), a transcriptional enhancer, was decreased. Also, our spatial transcriptomic results demonstrated that naïve and 3-day TAC hearts had fetal-gene–rich tissue domains that were enriched in pathways in extracellular matrix organization and tissue remodeling. As well, gene levels of glycolytic enzymes were higher in *Myh7*-positive than *Myh7*-negative domains.

Conclusions: Our data suggest that βMHC-expressed cardiomyocytes progress to pathological remodeling in the early stages of cardiac hypertrophy. In addition, the diverse glycolytic activity among cardiomyocytes might play a role in regulating gene expression via TEAD1 signaling.

1. Introduction

Cardiovascular disease is the leading cause of death globally. It claimed approximately 17.9 million lives in 2019 [1], and the number is expected to grow to 22.2 million by 2030 [2]. During the progression of heart disease, cardiac hypertrophy often initially occurs as a compensatory mechanism to reduce pressure overload in the heart and help maintain cardiac output and perfusion of vital organs. However, this compensatory response can fail over time, owing to accumulation of fibrotic tissue, insufficient angiogenesis, impaired cardiomyocyte (CM) contractile ability, and prevalence of mitochondrial dysfunction [3]. In response to diverse factors that increase the cardiac workload, such as exercise and valve disease, various signal transduction pathways are activated to induce adaptive or maladaptive cardiac growth (also called physiological or pathological cardiac remodeling/hypertrophy). The signaling pathways driving physiological and pathological cardiac hypertrophy have been intensively investigated [4–9]. As a result of these studies, the underlying mechanisms of pathological cardiac remodeling have been targeted by novel treatments that profoundly improve patient survival rates and reduce morbidity [10,11]. Despite this clinical success, some patients still progress to heart failure. An optimal treatment strategy for pathological cardiac remodeling and heart failure remains to be established.

Our current understanding of the signaling pathways underlying the development of cardiac hypertrophy has mostly been gained under the assumption that CMs respond uniformly to hypertrophic stimuli. Reprogramming of fetal genes (such as *Myh7* and *Nppa*) and changes in levels of calcium handling proteins (such as SERCA2a and Na(+)/Ca(2+) exchanger [NCX1]) are features of pathological remodeling. Nonetheless, their heterogeneous expression in pathological cardiac hypertrophy were reported decades ago [12–15]. As well, heterogeneity within CM

* Corresponding author at: Institute of Biomedical Sciences, Academia Sinica, 128 Academia Rd Sec 2, Nankang, Taipei 11529, Taiwan.
E-mail address: ccchen@ibms.sinica.edu.tw (C.-C. Chen).

http://dx.doi.org/10.1016/j.jmccpl.2022.100011
Received 8 May 2022; Received in revised form 24 May 2022; Accepted 16 June 2022

populations was recently demonstrated by single-cell RNA sequencing [16–20]. Despite the abundant information from single-cell transcriptomic studies, we do not know why fetal genes are heterogeneously expressed in the diseased heart and how the diverse gene profiles of cardiomyocytes may affect cardiac function. Because fetal genes are widely used markers for diseased hearts, we wondered whether fetal-gene–expressed CMs might be prone to pathological remodeling.

In this study, we used transverse aortic constriction (TAC) for 3 days to induce cardiac pressure overload in mice [21] and observed a subset of CMs with expression of β-myosin heavy chain (βMHC, encoded by *Myh7*) after TAC. To understand the pathophysiological role of this heterogeneous response, we profiled the transcriptomes and proteomes of βMHC-expressed and non-expressed cardiomyocytes in 3-day TAC hearts. βMHC-expressed CMs had a higher level of *Nppa* (another fetal gene) at the early stage of cardiac hypertrophy but were also enriched in transcripts and protein products of cardiomyopathy-associated genes. Another hallmark of pathological remodeling is the metabolic shift from fatty acid β-oxidation to glycolytic ATP production [22–27]. However, whether this phenomenon is heterogeneous among cells is not clear, nor is how early the metabolic shift occurs during the development of pathological cardiac hypertrophy. Here, we demonstrated that glycolytic activity was higher in βMHC-expressed than non-expressed CMs in 3-day pressure-overloaded hearts. The early inhibition of glycolytic flux could reduce the population of βMHC-expressed cardiomyocytes. Additionally, spatial transcriptomic analysis [28–32] revealed that fetal-gene–rich tissue domains were enriched in pathways in extracellular matrix (ECM) organization and tissue remodeling. Also, expression of glycolysis genes was higher in *Myh7*-positive than *Myh7*-negative tissue domains. Thus, our data describe a subpopulation of CMs that undergoes pathological remodeling before the heart becomes diseased. Moreover, the accumulation of pathological features in CMs may be associated with the progression of pathological cardiac hypertrophy.

2. Materials & methods

2.1. Animal model of cardiac hypertrophy

Eight- to 12-week-old adult male mice weighing 22–28 g were anesthetized (vaporized 1–1.5 % isoflurane) and subjected to pressure overload by TAC as described [21,33]. We used a 27G needle for aorta constriction. The yellow fluorescent protein (YFP)-βMHC mouse line was generated by Pandya et al. [14]. The coding sequence for YFP was inserted in the βMHC gene at the translational start site to generate a YFP-βMHC fusion allele that expresses YFP fused to the native βMHC protein. The YFP-βMHC mouse line was bred in 129 × 1/SvJ background. We used homozygous transgenic animals in this study. 2-Deoxy-D-glucose (2-DG) was intraperitoneally injected at 100 mg/kg/day daily. Besides, we used C57CL/6JNarl wild-type mice for spatial transcriptome. Animals were kept under specific pathogen-free conditions, and all procedures were approved by the Institutional Animal Care and Use Committee (IACUC) of Academia Sinica, Taiwan. The IACUC protocol complied with the Guide for the Care and Use of Laboratory Animals (Guide 2011, NIH) and followed the instructions of the Association for Assessment and Accreditation of Laboratory Animal Care, International, AAALAC.

2.2. Cardiac sections and spatial transcriptome

Hearts were harvested from 8-week-old mice and embedded in OCT, then immersed in 2-methylbutane pre-chilled by a liquid nitrogen bath. Cardiac sections of 10 μm were cryosectioned and placed on pre-chilled Visium spatial tissue optimization (TO) slides or gene expression (GE) slides. The procedure followed the manufacturer's user guide (10x Genomics). Tissue sections were permeabilized for 12 min to liberate RNA from cells, then first-strand cDNA was synthesized on-slide with oligo-dT primers, which were linked to the space barcode printed on the GE slide. The cDNAs were recovered from the GE slide and transferred to PCR tubes for second-strand synthesis, cDNA amplification, and Illumina library construction. Sequencing was performed by the NGS High Throughput Genomics Core at the Biodiversity Research Center, Academia Sinica (Taiwan). Libraries were sequenced with 100-bp paired-end reads using Illumina HiSeq 2500 System. The raw data were processed with Space Ranger v1.1.0 (10x Genomics) with default settings. The manual fiducial alignment was applied, and detection spots with tissue covering with >50 % were used for further analysis. The log-normalization was used to view feature expression normalized by UMI count, following the protocol of Seurat [34–36] and Scanpy [37]. The quantitative expression was computed as LogNorm(feature, barcode) = ln(10,000*(feature count/barcode count) + 1). The processed and analyzed data were visualized with Loupe Browser v4.1.0 (10x Genomics). The processed data were also analyzed by Partek Flow (Partek Inc.) with their single-cell analysis pipeline. The read counts were normalized by the counts per million (CPM) method and transformed to log2(CPM + 1). Gene-specific analyses were filtered with false discovery rate (FDR) < 0.01 and fold change >2. K-means clustering for the individual samples was automatically computed with k = 3–10.

2.3. Cardiomyocyte isolation

The procedure to isolate adult mouse cardiomyocytes was based on previous publications [38,39]. We used the Langendorff heart perfusion system for enzyme digestion in the heart. The heart was quickly removed and retrograde-perfused through the aorta at constant flow of 3 ml/min for 4 min at 37 °C with perfusion buffer containing 120.4 mM NaCl, 14.7 mM KCl, 0.6 mM KH_2PO_4, 0.6 mM Na_2HPO_4, 1.2 mM $MgSO_4{\cdot}7H_2O$, 10 mM Na-HEPES, 4.6 mM $NaHCO_3$, 30 mM Taurine, 10 mM BDM and 5.5 mM Glucose, pH 7.0. Then, the heart was perfused for 7 to 12 min with digestion solution containing collagenase B, collagenase D, and protease type XIV dissolved in perfusion buffer. The flaccid heart was removed from the cannula and the left ventricle was teased apart with forceps in KB buffer (85 mM K-glutamate, 30 mM K_2HPO_4, 5 mM sodium pyruvate, 0.5 mM EGTA, 20 mM taurine, 20 mM glucose, 5 mM creatine, 2 mM Na_2ATP, 5 mM $MgCl_2$, and 10 mM BDM). Tissues were further dissociated by using plastic transfer pipettes with different-size openings (1.5- and 1.0-mm diameters). The cardiomyocyte suspension was passed through a 250-μm cell strainer to obtain a single-cell suspension. Cardiomyocytes were pelleted at 20 rcf for 3 min to remove most of the other cell types, then cardiomyocytes were resuspended in KB buffer. The isolated cardiomyocytes were used immediately for cell sorting.

2.4. FACS and sample collection

Sorting was performed at the Academia Sinica Flow Cytometry Core on a BD FACSAria system with a 670/14 bandpass filter for propidium iodide (PI) and 530/30 bandpass filter for YFP. A 100-μm nozzle was used and PI-negative cardiomyocytes were collected for further application. For the RNA sample, cardiomyocytes were sorted into Invitrogen RNAlater Stabilization Solution (AM7020, ThermoFisher Scientific) and total RNA was extracted by using Trizol Reagent (15,596,018, ThermoFisher Scientific) or the RNAeasy Micro Kit (74,004, Qiagen). For protein samples, cardiomyocytes were sorted into KB buffer with additional protease inhibitor (AEBSF 2 mM, phosphoramidon 1 μM, bestatin 130 μM, E-64 14 μM, leupeptin 1 μM, aprotinin 0.2 μM, and pepstatin A 10 μM). Cardiomyocytes were pelleted at 600 rcf for 3 min and snap-frozen or immediately used for protein extraction.

2.5. Next-generation sequencing

Sequencing was performed at the NGS High Throughput Genomics Core at the Biodiversity Research Center, Academia Sinica (Taiwan). Total RNA was purified by using Trizol Reagent, and the quality of RNA was measured by Qubit assays (ThermoFisher Scientific) and Agilent 2100 Bioanalyzer. The RIN ratios ranged from 7.9 to 8.8. Total RNA was processed by using

the Illumina RNA library prep, and libraries were sequenced with 100 bp paired-end reads with the Illumina HiSeq 2500 System.

2.6. RNA sequencing data processing and identification of differentially expressed genes (DEGs)

Low-quality bases and reads were removed by using Trimmomatic v0.39. The processed reads were mapped to the mouse genome (GRCm38) by using Tophat v2.0.10 [40] and its embedded aligner Bowtie2 v2.1.0 [41]. The expression level (FPKM) of each gene was estimated by using Cufflinks v2.1.1 [42]. Genes with FPKM ≥ 1 in two or more samples were considered expressed and selected for further analysis. To compare the FPKMs of the selected genes across samples in a set of transcriptomes, the upper quartile normalization procedure was applied. The nonparametric method of NOIseq [43] was used to identify DEGs between two samples. The q value (differentially expression probability) in the method was set to 0.7, because the genes in the dataset with $q > 0.7$ had at least a 2.3-fold change in FPKM between the two samples.

2.7. Quantitative RT-PCR

The first-strand cDNA was synthesized by using SuperScript III Reverse Transcriptase (18,080, Thermo Fisher Scientific Inc.). qRT-PCR was performed on an Applied Biosystems 7500 real-time system with Power SYBR® Green Master Mix (4,367,659, Thermo Fisher Scientific Inc.). Primers are listed in Supplementary Table 1.

2.8. Proteomics

Cardiomyocytes were lysed in 1 % SDS in 100 mM HEPES buffer with proteinase inhibitor, and protein concentrations were determined by a Bio-Rad detergent compatible (DC) protein assay. In all, 50 μg protein was reduced by 2 mM TCEP, alkylated by 5 mM MMTS, precipitated and washed by cold acetone. The purified protein extracts were digested to peptides by Lys-C protease, followed by overnight trypsin. Then, the peptides were labeled by using TMT10-plex Mass Tag Labeling Kits and Reagents (Thermo Fisher Scientific Inc.). The labeling efficiency was checked with LC-MS/MS before combining 10 TMT-labeled peptides. The analysis of TMT-labeled peptides was modified from a previous method [44]. Briefly, the mixed TMT peptides were fractionated with hydrophilic interaction liquid chromatography (HILIC). The labeled peptides in each HILIC fraction were analyzed by using Waters nanoACQUITY UPLC coupled to an Orbitrap Fusion mass spectrometer. The acquired tandem mass spectra were processed by using Proteome Discoverer v2.2 and searched by using Mascot algorithms against the Uniprot mouse database (UniProt Knowledgebase release 2018_10, 17,058 sequences). The mass tolerance of precursor and fragment ions were 10 ppm and 0.02 Da. Oxidation of methionine, methylthio of cysteine and deamidation of asparagine/glutamine were set as variable modifications. TMT tags on the peptide N-terminus/lysine was set as a fixed modification. Target-decoy searching was used to estimate the protein FDR, and 1 % or 5 % FDR was set as high or medium confidence, respectively. Quantification of TMT-labeled peptides was performed by using the reporter ions quantifier of Proteome Discoverer, and the normalization mode was total peptide amount. The co-isolation threshold was <50 %, and average reporter S/N threshold was >10. Paired Student *t*-test was used to identify differentially expressed proteins between two cardiomyocyte groups ($p < 0.05$).

2.9. Pathway analysis

The identified DEGs were analyzed by using IPA (Qiagen Inc., https://www.qiagenbioinformatics.com/products/ingenuity-pathway-analysis) [45] or Metascape (http://metascape.org) [46] for gene ontology analysis, functional analysis, and networks. The detected 11,842 genes from our RNA-seq data were used as background gene set for gene ontology analysis. Gene Set Enrichment Analysis (GSEA) was used to compute and determine the active or inactive state of an a priori-defined set of genes [47,48].

2.10. Western blotting

Proteins were equally loaded on SDS-PAGE with T-Pro EZ gel 10 % (T-Pro Biotechnology) for western blot analysis. Anti-Myosin (Skeletal, Slow), clone NOQ7.5.4D (1:2000, Sigma-Aldrich) was used to detect βMHC. Anti-Hexokinase I (HK1; clone C35C4), anti-HK2 (clone C64G5), anti-phosphofructokinase (PFKP) (clone D4B2), anti-phosphoglycerate mutase 1 (PGAM1) (clone D3J9T), and anti- TEA domain family member 1 (TEAD1) (D9X2L) (all 1:1000 dilution) were from Cell Signaling Technology. Anti-NCX1 (clone C2C12) (1:1000 dilution) was purchased from Genetex. Anti-SERCA2 ATpase (clone 2A7-A1) (1:1000 dilution) was purchased from Abcam. HRP-conjugated GAPDH antibody (1:5000, Proteintech Group, Inc.) was used to detect GAPDH. Total protein amount was calculated from Coomassie blue-stained PVDF membranes for normalization. The enhanced chemiluminescence (ECL) method was used to detect individual proteins on a Fujifilm Luminescent Image Analyzer System (FUJIFILM Corp.). The original images were analyzed by using ImageJ for quantification.

2.11. Glycolysis enzyme activity

The Sigma-Aldrich Hexokinase Colorimetric Assay Kit (MAK091) and GAPDH Activity Assay Kit (MAK277) were used to measure HK and GAPDH activity, respectively.

2.12. Data availability

The Illumina reads were deposited in the Sequence Read Archive under https://www.ncbi.nlm.nih.gov/sra/PRJNA661625 (accession no. PRJNA661625). The mass spectrometry proteomics data were deposited to the ProteomeXchange Consortium via the PRIDE [49] partner repository with the dataset identifier PXD021671 (Username: reviewer_pxd021671@ebi.ac.uk; Password: e4dmF2fS).

2.13. Statistics

Data are presented as mean with SD. Statistical comparisons involved using paired Student *t*-test to compare βMHC-negative and -positive samples from the same heart, unpaired Student *t*-test to compare two independent samples, and one-way ANOVA followed by multiple comparisons to compare multiple groups. $P < 0.05$ was considered statistically significant. The data were analyzed and graphed by using GraphPad Prism 9.

3. Results

3.1. βMHC re-expressed in a subset of CMs after pressure overload

Many studies have investigated changes in the late stages of cardiac hypertrophy to address the transition from compensatory hypertrophy to failure heart. Nevertheless, levels of some pathological markers, such as *Myh7* (a fetal gene), change in the early stage of cardiac hypertrophy. In the current study, we sought to investigate the changes in CMs at the initial stage of pressure-overload-induced cardiac remodeling. Taking advantage of a transgenic mouse line that expresses yellow-fluorescent protein fused to the native βMHC (YFP-βMHC), we easily identified *Myh7* (encodes βMHC) re-expression by tracking YFP [14]. We induced cardiac pressure overload in mice by TAC and found that a subset of CMs expressed YFP-βMHC (Fig. 1A: LV section, YFP CMs in green). We next isolated adult left ventricular CMs and used fluorescence-activated cell sorting (FACS) to separate YFP-βMHC negative (YFP^-) and positive (YFP^+) CMs from 3-day TAC hearts. YFP expression was confirmed by fluorescent microscopy and βMHC expression by immunoblotting (Fig. 1A). The proportion of YFP^+ CMs was significantly induced after 3-day TAC and was maintained

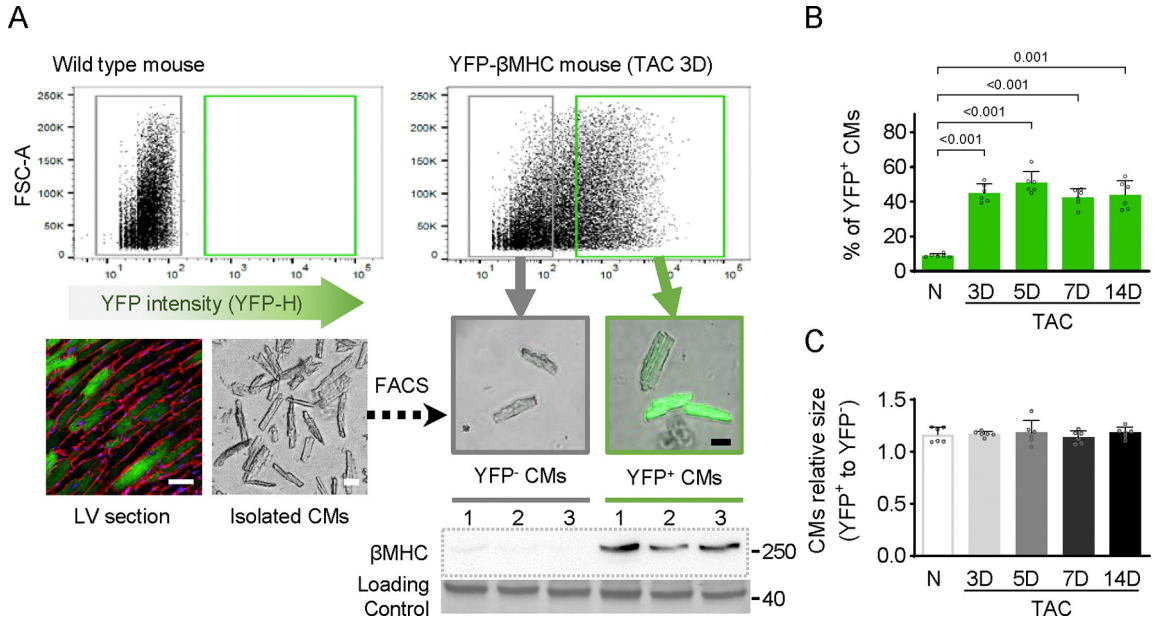

Fig. 1. Number of YFP$^+$ CMs increases after 3-day TAC and YFP$^+$ CMs are larger than YFP$^-$ CMs. (A) Left ventricular (LV) cardiac section of a 3-day TAC heart shows wheat germ agglutinin (WGA)-outlined CMs in red and YFP-βMHC CMs in green. YFP$^-$ CMs and YFP$^+$ CMs were collected from isolated CMs with an FACSAria IIIu cell sorter, according to YFP signal intensity. βMHC expression is confirmed by western blot analysis. (B) Proportion of YFP$^+$ CMs after TAC. (C) Relative size of YFP$^+$ to YFP$^-$ CMs. Data are mean ± SD. One-way ANOVA, followed by multiple comparisons, $n = 6$ per group. Scale bars: 50 μm. Abbreviations: TAC: transverse aortic constriction; LV: left ventricular; CMs: cardiomyocytes; YFP$^-$ or YFP$^+$ CMs: YFP-βMHC negative or positive CMs; FACS: fluorescence-activated cell sorting.

thereafter (Fig. 1B). In addition, flow cytometry revealed that YFP$^+$ CMs were larger than YFP$^-$ CMs at all times (Fig. 1C). The size of left ventricular CMs was slightly increased after 3-day TAC and increased even more with continued pressure overload (Supplementary Fig. 1). Both YFP$^-$ and YFP$^+$ CMs significantly increased in size after pressure overload for 7 days. Thus, CMs in the same heart can respond differently to hypertrophic stimuli.

3.2. YFP$^-$ and YFP$^+$ CMs of 3-day TAC hearts have distinct gene profiles

Because fetal gene reprogramming, a pathological marker, occurred in a subset of CMs at the beginning of pressure overload-induced cardiac hypertrophy and persisted during pathological remodeling, we wondered whether early induction of fetal gene re-expression is important for cardiac physiology. To know the differences between fetal gene-expressed and non-expressed CMs in early cardiac hypertrophy, we used transcriptomic analysis of YFP$^-$ and YFP$^+$ CMs. We subjected five YFP-βMHC mice to 3-day TAC and performed transcriptional profiling on sorted CMs by next-generation sequencing (RNA-seq). The total number of differentially expressed genes (DEGs) in each of the five mice was 371, 292, 386, 393, and 232. We examined DEGs among five samples to select genes with the same expression trends for further validation and analysis (Supplementary Table 2). We first analyzed the selected DEGs by Qiagen Ingenuity Pathway Analysis and found that eukaryotic initiation factor 2 signaling was the most enriched pathway in YFP$^-$ CMs. In contrast, ephrin receptor and neuregulin signaling were enriched in YFP$^+$ CMs. Ephrin receptor signaling and neuregulin signaling have been found involved in cardiac disease [50–54], which suggests that YFP$^+$ CMs displayed more pathological features than did YFP$^-$ CMs.

We also validated our genes of interest by quantitative RT-PCR (qRT-PCR) with a new batch of left ventricular CM samples. The relative gene levels of YFP$^+$ to YFP$^-$ CMs by qRT-PCR were positively correlated with the results from RNA-seq (Supplementary Fig. 2), which suggests that the identified gene expression changes by RNA-seq are reproducible and reflect actual gene profiles in the TAC samples. Notably, both RNA-seq and qRT-PCR results showed that YFP$^+$ CMs had higher expression of another fetal gene, *Nppa* (Fig. 2A and B). We also observed signs of pathological remodeling by the elevated expression of genes including *Xirp2* [55–57], *Itga5* [58,59], and *Tead1* [60] in YFP$^+$ CMs (Fig. 2A). The qRT-PCR results confirmed higher expression of *Xirp2*, *Itga5*, and *Tead1* in YFP$^+$ CMs (Fig. 2B).

Next, we performed gene ontology (GO) analysis of selected DEGs by using Metascape [46]. Ribosome function and oxidative phosphorylation were most enriched in YFP$^-$ CMs (Fig. 2C, upper panel). However, genes involved in actin filament-based processes and intermediate filament cytoskeleton organization were highly expressed in YFP$^+$ CMs (Fig. 2C, lower panel). Additionally, YFP$^+$ CMs had enriched pathways related to hypertrophy cardiomyopathy and pathological cardiac remodeling, such as MAPK [61] and SMAD signal transduction [62–64]. YFP$^+$ CMs were enriched in pathways involved in regulation of the glycolytic process (highlighted in the lower panel of Fig. 2C). Therefore, YFP$^+$ CMs expressed more pathology-related factors at the beginning of cardiac hypertrophy. Also, GO network analysis revealed that YFP$^-$ and YFP$^+$ CMs possessed distinct biological processes (Fig. 2D), which supports the different responses of CMs in the same pressure-overloaded heart.

3.3. YFP$^+$ CMs in 3-day TAC hearts favor glycolysis

To better understand the functional profiles of YFP$^-$ and YFP$^+$ CMs, we used Gene Set Enrichment Analysis (GSEA) [47,48] of our RNA-seq dataset. The top 20 enrichments are listed in Supplementary Table 3. The fatty acid metabolic process was enriched in YFP$^-$ CMs, and the glycolytic process was enriched in YFP$^+$ CMs (Fig. 2E), which agrees with the GO analysis of selected DEGs. Besides transcriptional profiles, we examined protein levels of glycolytic enzymes in YFP$^-$ and YFP$^+$ CMs. The immunoblotting results showed higher expression of glycolytic enzymes in YFP$^+$ than YFP$^-$ CMs (Fig. 3A and B).

The enzyme activity assays of hexokinase (HK, the rate-limiting enzyme of glycolysis) and glyceraldehyde-3-phosphate dehydrogenase (GAPDH, the key enzyme regulating glycolytic flux) showed that both HK and GAPDH activities were higher in YFP$^+$ than YFP$^-$ CMs (Fig. 3C). A metabolic shift from oxidative phosphorylation to glycolysis is a key

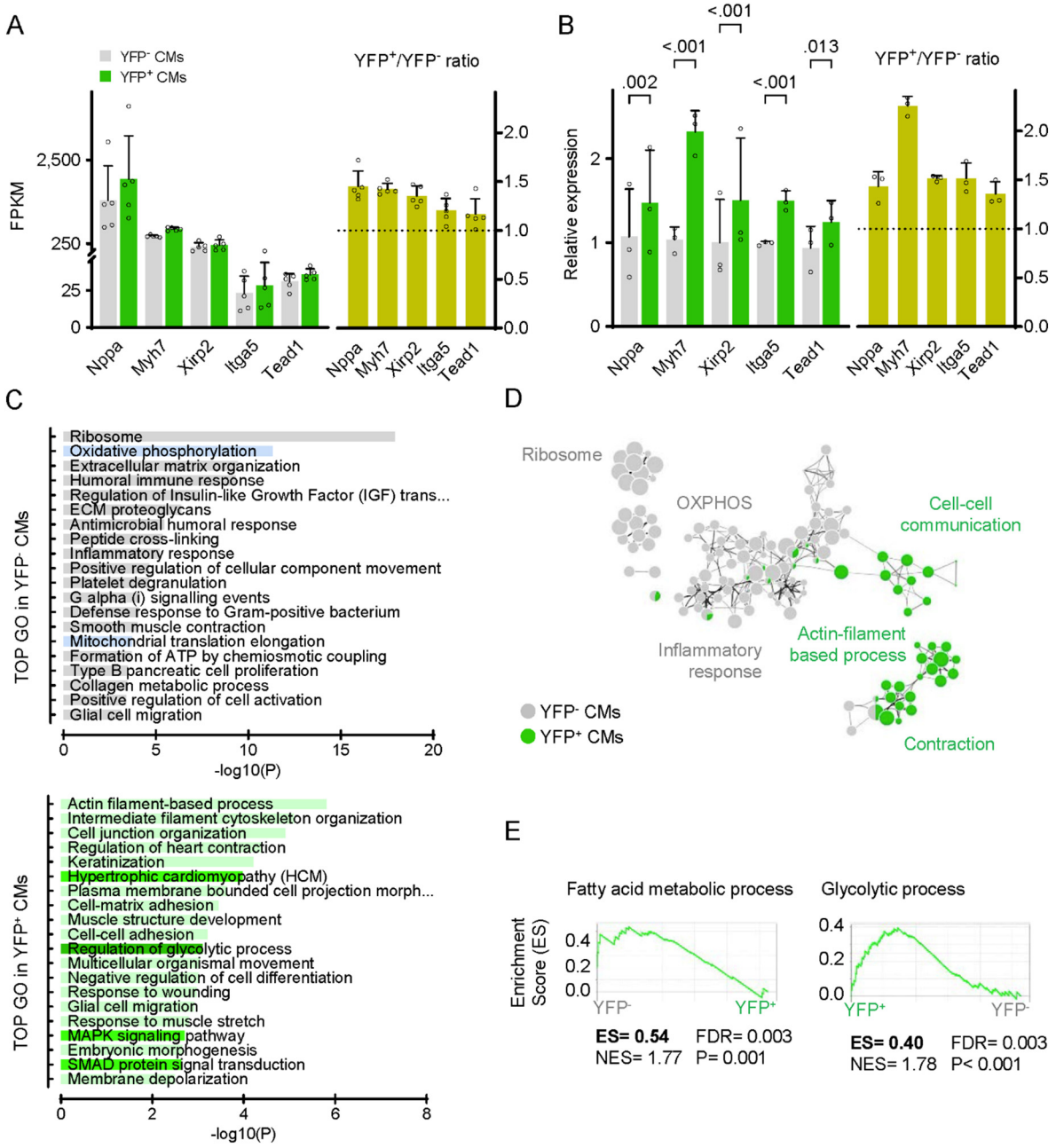

Fig. 2. Transcriptomic analysis reveals diverse enriched biological processes in YFP$^-$ and YFP$^+$ CMs. Gene expression analysis by (A) differentially expressed gene analysis of RNA-seq results; expression levels are indicated by FPKM ($n = 5$) and (B) mRNA relative quantification by qRT-PCR (paired Student *t*-test, $n = 3$). Data are mean ± SD. (C) Top clusters with representative transcriptomic enriched terms identified by Metascape. (D) Gene Ontology network analysis of transcriptomic data. (E) Gene Set Enrichment Analysis of RNA-seq results. Abbreviations: CMs: cardiomyocytes; YFP$^-$ or YFP$^+$ CMs: YFP-βMHC negative or positive CMs; GO: gene ontology; ES: enrichment score; NES: normalized enrichment score.

characteristic of pathological remodeling, which is thought to occur because CMs increase glucose utilization to meet higher energy demands under stress conditions [22–27]. Nonetheless, our findings indicate that YFP$^+$ CMs might undergo a metabolic shift even at the early stages of pressure overload-induced cardiac remodeling.

Because modulation of the proteome directly affects cellular physiology, we further used multiplex relative protein quantification to profile protein expression differences between YFP$^-$ and YFP$^+$ CMs. We identified 87 proteins that were highly expressed in YFP$^-$ CMs and 84 proteins that were highly expressed in YFP$^+$ CMs from 3-day TAC hearts (Supplementary Table 4). GO analysis of these elevated proteins revealed that YFP$^-$ CMs were enriched in cellular respiration and mitochondrial-associated processes (Fig. 3D, left panel). In contrast, YFP$^+$ CMs were enriched in pathways related to pathological remodeling, such as dilated cardiomyopathy and the calcineurin-NFAT signaling cascade (Fig. 3D, right panel). In addition, we observed an enrichment of the glycogen metabolic process in YFP$^+$ CMs (highlighted in the right panel of Fig. 3D). Myocardial glycogen is an essential source of glucose for glycolysis in the heart, so the enriched glycogen metabolism in YFP$^+$ CMs implies that the glycolytic activity could be higher in YFP$^+$ than YFP$^-$ CMs.

Moreover, our proteomic analysis showed that several enzymes involved in glycolysis were elevated in YFP$^+$ CMs (Fig. 3E). Similar to our transcriptomic analysis, GO network analysis of proteomic results showed that the enriched biological processes were divergent in YFP$^-$ and YFP$^+$

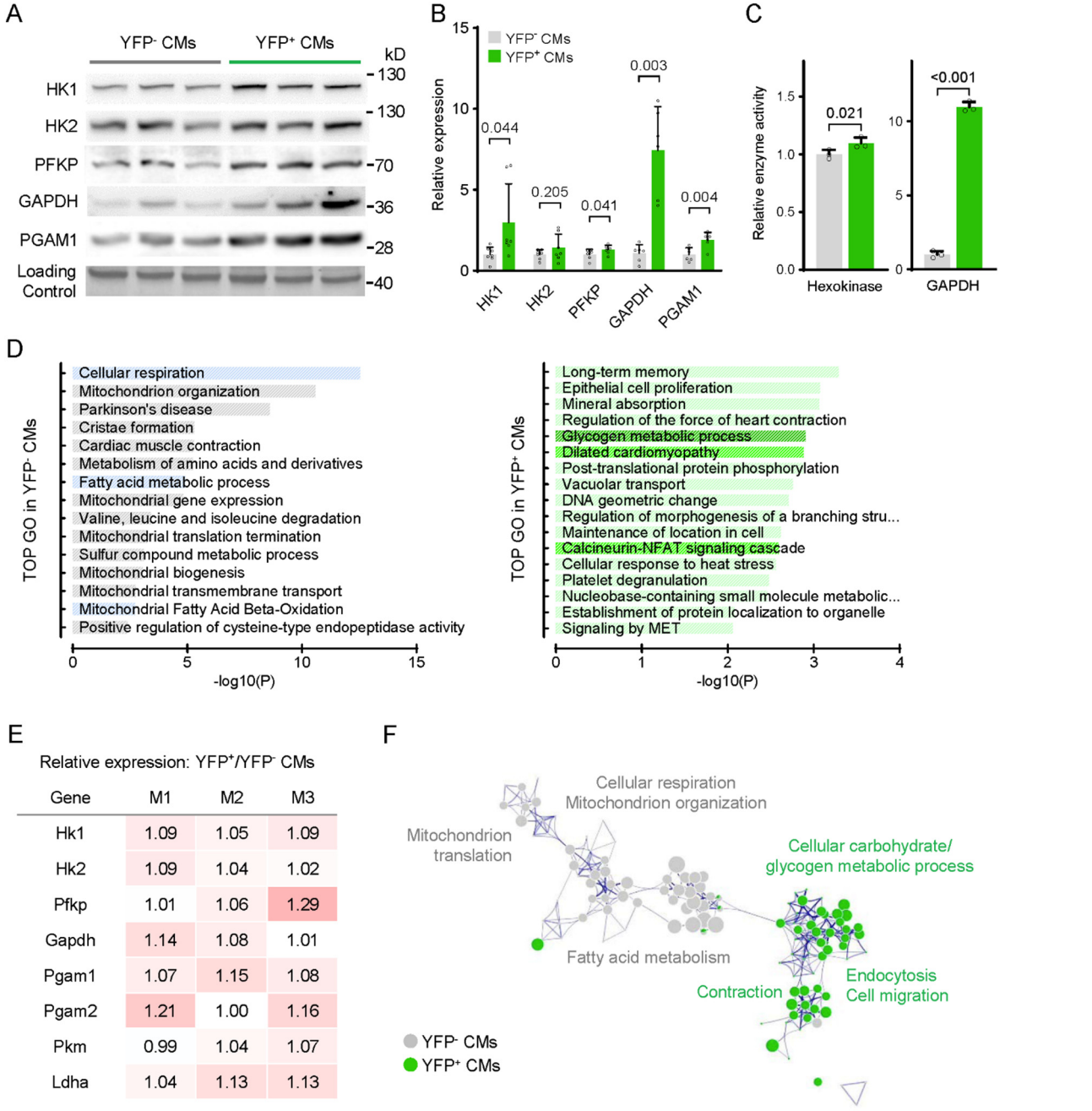

Gene	M1	M2	M3
Hk1	1.09	1.05	1.09
Hk2	1.09	1.04	1.02
Pfkp	1.01	1.06	1.29
Gapdh	1.14	1.08	1.01
Pgam1	1.07	1.15	1.08
Pgam2	1.21	1.00	1.16
Pkm	0.99	1.04	1.07
Ldha	1.04	1.13	1.13

Fig. 3. Glycolytic pathway is more active in YFP$^+$ than YFP$^-$ CMs. (A) Representative western blots of glycolysis enzymes and (B) quantification ($n = 6$). (C) Enzyme activity assay of hexokinase and GAPDH ($n = 3$). Paired Student *t*-test. Data are mean ± SD. (D) Top clusters with representative proteomic enriched terms identified by Metascape. (E) Proteomic analysis of enzymes involved in glycolysis and relative ratios of expression levels in YFP$^+$ to YFP$^-$ CMs. (F) Gene Ontology network analysis of proteomic data. Abbreviations: CMs: cardiomyocytes; YFP$^-$ or YFP$^+$ CMs: YFP-βMHC negative or positive CMs; GO: gene ontology.

CMs (Fig. 3F). Taken together, YFP$^+$ CMs could be in a more pathological condition, expressing pathology-associated molecules and preferring the glycolytic pathway, as compared with YFP$^-$ CMs.

3.4. Inhibition of glycolysis reduces the proportion of YFP$^+$ CMs in 3-day TAC hearts

As discussed above, the metabolic shift is thought to be a feature in the later stages of cardiac remodeling. However, our results demonstrate that a subset of CMs expressed glycolytic enzymes and had high enzyme activity of the initial step of glycolysis. Thus, we wondered whether the early modulation of glycolysis could regulate *Myh7* re-expression at the early stage of pressure overload-induced cardiac hypertrophy. To test this, we treated 3-day TAC mice with 2-deoxy-glucose (2-DG, 100 mg/kg/day) daily. 2-DG is a competitive inhibitor of HK and widely used for inhibiting glycolytic processes. This low dose of 2-DG has been shown to sufficiently inhibit glycolysis without apparent systemic side effects [65].

We used flow cytometry to evaluate the number of βMHC-expressed CMs from 3-day TAC YFP-βMHC mice and found reduced proportion of YFP$^+$ CMs in the 2-DG–treated group as compared with the saline control (Fig. 4A). We then examined the mRNA levels by qRT-PCR in CMs of control and 2-DG–treated mice to determine whether the global inhibition of glycolysis affected pathology-associated pathways. These pathways include calcium homeostasis, mechanical sensing, and ECM organization. 2-DG treatment did not significantly change ECM-related gene levels as compared with the control (Fig. 4B), which suggests that this glycolytic

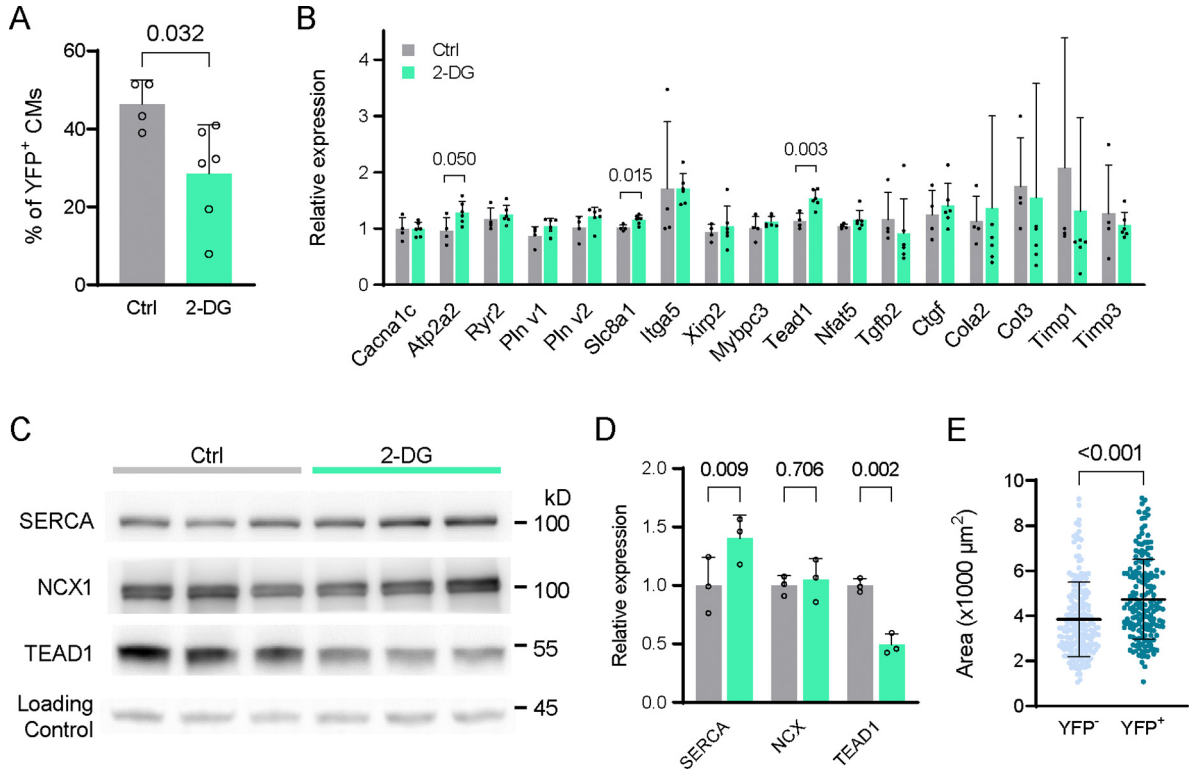

Fig. 4. 2-DG treatment reduces the number of YFP$^+$ CMs in 3-day TAC hearts. (A) Proportion of YFP$^+$ CMs after TAC/2-DG for 3 days ($n = 4$ in control group and $n = 6$ in 2-DG group). (B) Gene levels assessed by qRT-PCR. (C) Protein levels assessed by western blot analysis and (D) quantification ($n = 3$). (E) Cell size of isolated YFP$^-$ and YFP$^+$ CMs. Student *t*-test. Data are mean ± SD. Abbreviations: Ctrl: control; CMs: cardiomyocytes; YFP$^-$ or YFP$^+$ CMs: YFP-βMHC negative or positive CMs; GO: gene ontology.

inhibition barely affects ECM organization in the early stages of cardiac remodeling.

However, we observed induced *Atp2a2* (encodes SERCA2a) and *Slc8a1* (encodes NCX1) mRNA levels in the 2-DG group (Fig. 4B). We further confirmed the induction of SERCA2a at the protein level in the 2-DG group. However, NCX1 level did not differ from the control level (Fig. 4C and D). Hence, glycolytic flux might modulate calcium homeostasis by regulating calcium transporter expression in CMs. The changed level of SERCA2a could be independent of βMHC expression, but also the changed calcium homeostasis might signal fetal-gene reprogramming in CMs.

The mRNA level of *Tead1* (also known as transcriptional enhancer factor 1) was increased but the protein level was reduced in the 2-DG group (Fig. 4B to D). TEAD1 could positively regulate *Myh7* expression [60], and its transcriptional activity could be regulated by glycolysis [66]. The decreased protein level of TEAD1 reflects the reduced proportion of YFP$^+$ CMs in 2-DG–treated TAC hearts. TAC may generally induce *Myh7* reprogramming via upregulated *Tead1* mRNA expression, but the inhibition of glycolysis may suppress TEAD1 activity via the translational control, which exerts an acute effect on βMHC expression in the early stages of cardiac hypertrophy. Although the number of YFP$^+$ CMs was reduced by 2-DG treatment, YFP$^+$ CMs were still larger than YFP$^-$ CMs (Fig. 4E). Collectively, interrupting the initiation step of glycolysis by 2-DG reduced the number of βMHC–re-expressed CMs and affected Tead1 and calcium handling molecule expression. Thus, the glycolytic status could directly modulate βMHC expression via TEAD1 signaling.

3.5. Spatial transcriptome reveals high glycolysis activity and cell–cell interactions in Myh7-rich cardiac microdomains

We investigated the cell properties of YFP$^-$ and YFP$^+$ CMs. Transcriptomic analysis showed that cell adhesion or ECM organization were both enriched in YFP$^-$ and YFP$^+$ CMs, but the enriched molecules differed. Also, the 2-DG data (Fig. 4) showed that SERCA2a level changed in CMs, which implies that glycolytic status affects dynamic calcium handling. Furthermore, from our RNA-seq data, several DEGs were classified in the ion channel category and included *Cacna1g*, *Cacna1c*, and *Casq1*. DEG analysis also revealed higher growth-factor and cytokine levels in YFP$^+$ than YFP$^-$ CMs (Supplementary Fig. 3). This differential gene expression of CMs might modulate the phenotype of their adjacent cells. Hence, we used Visium Spatial Gene Expression to assess gene profiles in cardiac sections. This technique detects gene expression with spatial information from the designed detection spots (Supplementary Fig. 3).

The detection spots on a Visium gene expression slide were 55 μm in diameter, so each spot is expected to sample a tissue domain with multiple cells. We collected cardiac sections from naïve and 3-day TAC hearts and detected between 57 and 6720 genes in each spot from a 10-μm-thick cross-sections. The median detected genes per spot (tissue domain) was 2732. Then, we performed K-means clustering (K = 3 to 10) based on the gene profiles of tissue domains and found four tissue domain clusters in the naïve sample (Fig. 5A, a-naïve). The three TAC samples had 8, 10, 6 clusters each (Fig. 5A, b-, c-, and d-TAC). There were only two dominant tissue domain clusters in naïve and TAC samples. When we performed a biomarker analysis of these clusters, we found that fetal genes such as *Myh7* and *Nppa* were co-identified in one of the dominant clusters of each sample.

Next, we analyzed GO enrichment of biomarkers in these fetal-gene–rich tissue domain clusters from naïve and TAC samples. Biomarkers of these tissue domains showed common molecular functions, including fibronectin binding, signaling receptor regulator activity, and cell adhesion molecule binding (Fig. 5B). Notably, these fetal-gene–rich tissue domains from TAC samples were enriched in molecules with functions including ECM organization, growth factor binding, and calcium ion binding. In addition to molecular function analysis, GO analysis of biological processes showed that fetal-gene–rich domains shared the same pathways between naïve and TAC samples, such as tissue remodeling, muscle structure development, and ECM organization (Fig. 5C). Further enriched molecular functions were pathways associated with cell–cell interactions in fetal-gene–rich tissue domains of TAC hearts. Together with transcriptomic and

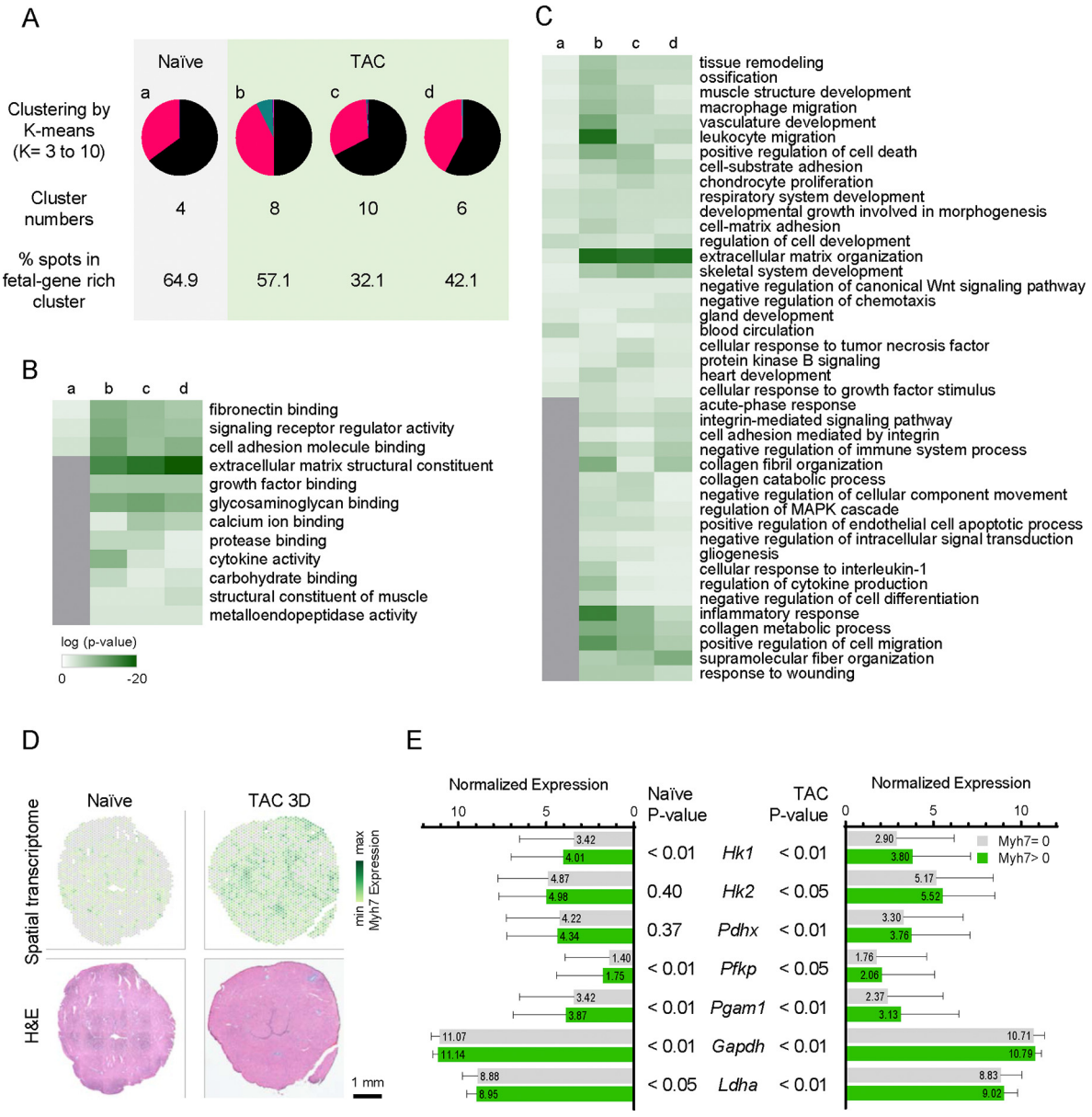

Fig. 5. Spatial transcriptomic analysis reveals fetal-gene–rich tissue domain clusters in naïve and 3-day TAC hearts. (A) K-means clustering result for naïve or TAC hearts by pie chart. (B) Gene Ontology (GO) analysis of molecular functions of biomarkers in fetal-gene–rich cluster of each sample. (C) GO analysis of biological processes of biomarkers in fetal-gene–rich cluster of each sample. (D) Spatial gene expression of *Myh7* and the H&E staining of naïve and 3-day TAC hearts. (E) Glycolysis-related genes in tissue domains with or without *Myh7* expression. Left panel is naïve sample and right panel is TAC sample. Data are mean ± SD and mean values are annotated. *P*-values are from Student *t*-tests comparing domains with or without *Myh7* expression for indicated genes. Abbreviations: TAC: transverse aortic constriction. GO: gene ontology. H&E: hematoxylin and eosin stain.

proteomic analysis of YFP$^-$ and YFP$^+$ CMs, these results indicate that fetal-gene–expressed CMs might regulate ECM formation via growth-factor/cytokine signaling in the pressure-overloaded hearts.

Spatial transcriptomic analysis demonstrated diverse levels of *Myh7* among tissue domains of the naïve sample, and significant induction of *Myh7* was detected in cardiac sections of 3-day TAC hearts (Fig. 5D). Moreover, even in naïve samples, mRNA levels of glycolytic enzymes were higher in tissue domains with than without *Myh7* expression (Fig. 5E, left panel). These data demonstrate that intrinsic glycolytic activity is positively correlated with *Myh7* expression. After pressure overload for 3 days, these enzyme differences between *Myh7*-negative and -positive domains became more apparent (Fig. 5E, right panel). Thus, short-term pressure overload could modulate glycolytic activity and might further regulate the fetal-gene expression and cellular functions. Also, the pre-existing differences in naïve CMs might explain the different responses of CMs in the pressure-overloaded hearts.

4. Discussion

Heterogeneous fetal-gene re-expression among CMs in diseased hearts has been observed for more than a decade; however, its role in the progression of cardiac hypertrophy to heart failure is unknown. To understand the biological meaning of CMs with fetal gene expression in the early stage of cardiac remodeling, we grouped CMs into two populations by βMHC expression. Our multi-omics analyses revealed diverse gene profiles between these two CM groups. Notably, the βMHC-positive CM population was enriched in genes in biological processes related to pathological remodeling, such as hypertrophy cardiomyopathy and the calcineurin-NFAT signal

cascade. CMs without βMHC expression were enriched in pathways in oxidative phosphorylation and fatty acid metabolic process. In addition, the omics and biochemical results demonstrated that glycolytic activity was enriched in βMHC-positive CMs of 3-day TAC hearts. Fetal-gene reprogramming, activation of the calcineurin-NFAT pathway, and metabolic shift from fatty acid metabolism to glycolysis are known features of pathological cardiac hypertrophy. Therefore, our results support that CMs with βMHC expression undergo pathological remodeling, even in the early stages of pressure overload-induced cardiac hypertrophy.

Single-cell transcriptomic studies demonstrated the heterogeneity of CMs in normal or diseased hearts [16–20], but the physiological effects of CM heterogeneity remain unknown. For example, Ren et al. studied the progression of pressure overload-induced cardiac hypertrophy and identified 10 CM subtypes, grouping them into four clusters by their transcriptome similarities. However, the authors explained little about the physiological relations between heterogeneous CMs and turned their focus to subtype switching of macrophages [20]. Therefore, we performed GO analysis on DEGs of their *Myh7*-high expressing CMs (logTPM ≥ 3). Since we could not fairly judge the cut-off of logTPM for βMHC-negative CMs, we first compared *Myh7*-high with *Myh7*-negative to see the enriched genes and pathways in *Myh7*-high expressing CMs. GO analysis revealed that *Myh7*-high expressing CMs enriched in pathways of cardiac morphological changes, such as cardiac muscle cell development, regulation of sarcomere organization, and cardiac muscle hypertrophy. Besides, metabolic pathways, such as carbon metabolism, glycogen metabolic process, and NADH metabolic process, were also enriched in *Myh7*-high expressing CMs (Supplementary Fig. 4). Collectively, we found some common enriched pathways in Ren's *Myh7*-high expressing CMs and our YFP^+ CMs.

The difficulty in explaining the heterogeneity of CMs could be due to limited knowledge regarding functional subtypes and genetic markers. Here, we grouped CMs according to βMHC re-expression, a marker of diseased hearts, to gain insight into their physiological meaning. We assayed the transcriptomic and proteomic differences between βMHC-expressed (YFP^+) and non-expressed (YFP^-) CMs. YFP^+ CMs of 3-day pressure-overloaded hearts showed elevated levels of *Tgfb2* and *Ctgf* (Supplementary Fig. 3A). Also, spatial transcriptomic results demonstrated that ECM organization pathways were more active in fetal-gene–rich cardiac microdomains than other domains without fetal-gene enrichment (Fig. 5B and C). Collectively, these results might explain the association between early βMHC expression and later fibrotic tissue formation [14], in which YFP^+ CMs might express growth factors or cytokines to enhance ECM organization during pressure overload-induced cardiac remodeling.

Additionally, we found HK activity higher in YFP^+ than YFP^- CMs, and treatment with 2-DG (the HK inhibitor) could decrease the number of YFP^+ CMs in pressure-overloaded hearts. HK metabolizes glucose to glucose 6-phosphate. This metabolite functions in glycolytic flux and also in the hexosamine biosynthetic pathway (HBP) and the pentose phosphate pathway. We also detected a higher level of *Gfpt1* (a rate-limiting enzyme of HBP) in the transcriptome of YFP^+ than YFP^- CMs, which implies elevated HBP signaling in YFP^+ CMs. Furthermore, chronic activation of HBP could trigger pathological cardiac remodeling [67]. As well, decreased β-adrenergic response in βMHC-expressed CMs was previously reported in 4-week TAC hearts [68]. However, YFP^- CMs showed more expression of factors in fatty acid metabolism, oxidative phosphorylation, ribosome, and mitochondrial-related components. These results resembled the Nomura et al. findings in their single-cell RNA transcriptomic study of sham (TAC control) hearts [19]. These reports further support our idea that YFP^+ CMs display more pathological features than do YFP^- CMs in the early stage of cardiac hypertrophy. The accumulation of these features might result in CM dysfunction over time.

Because YFP^+ CMs expressed higher levels of glycolytic enzymes than did YFP^- CMs, we further inhibited the initial step of glycolysis by 2-DG treatment and found reduced number of YFP^+ CMs in the 3-day TAC hearts. Also, CMs of 2-DG/TAC hearts had different expressions of TEAD1 and SERCA2a as compared with control CMs. Glycolysis can regulate the transcriptional activity of TEAD1 [66] and also modulates calcium homeostasis in cat atrial myocytes [69] and cancers [70]. Briefly, the intermediates of glycolysis could directly interact with calcium transporters or indirectly regulate their activity by GlcNAcylation and redox homeostasis. Also, the interplay between metabolism and epigenetic regulation was demonstrated in physiological and pathological conditions [71]. Angrisano et al. reported that epigenetic modification of *Atp2a2* and *Myh7* promotor regions regulated their expression in pressure overload-induced cardiac hypertrophy [72]. So, we reasoned that glycolytic flux modulates TEAD1 activity to affect βMHC expression and regulates SERCA2a expression to affect calcium homeostasis in CMs of 3-day TAC hearts. At the same time, glycolysis could be involved in epigenetic regulation of gene expression. Therefore, inhibition of glycolysis by an HK inhibitor probably prevents βMHC re-expression via diverse signaling pathways. Here we report one possible interplay between glycolytic flux, TEAD1, βMHC, and SERCA2a in CMs at the early stage of cardiac hypertrophy.

Adult CMs are terminally differentiated cells; hence, the diversity of gene expression profiles between CMs can be determined soon after birth. Previous single-cell transcriptomic analyses demonstrated cardiac cell diversity during development [16,17], and our spatial transcriptomic results also reveal a fetal-gene–rich tissue domain cluster in the naïve heart. The data from embryonic and adult naïve hearts suggest that CMs have different intrinsic properties, which results in diverse responses under stress. Whether any intrinsic factor determines the fate of CMs throughout life is an interesting question.

One drawback of our transcriptomic analysis is that we treated the sample as five individuals and analyzed their DEGs by NOIseq. To get a more robust gene list, we performed differential analysis by DEseq2 for all five mice in one DEGs analysis to account for biological variation between animals. We identified 635 DEGs in YFP^- CMs and 657 in YFP^+ CMs (Supplementary Fig. 5A). We performed GO analysis by Metascape as what we did for NOIseq results. There are common enriched pathways of DEseq2 and NOIseq results for YFP^- CMs and YFP^+ CMs (Supplementary Fig. 5B and 5C). These data provided additional support for our findings (Fig. 2).

In summary, we assessed the biological meaning of heterogeneity among CMs by comparing the transcriptome and proteome of βMHC-expressed CMs and non-expressed CMs at the early stage of hypertrophic response. CMs responded to pathological stimuli differently and pathological features were simultaneously enriched in βMHC-expressed CMs. Moreover, we used conventional experiments to support the findings of our omics data both in vitro and in vivo. Our approaches shed new light on the physiological relevance of CM heterogeneity in the same heart.

CRediT authorship contribution statement

H.-h.Y., M.-Y.L., and C.-C.C. designed the research. H.-h.Y., Y.-W.C., and Y.-H.C. performed the experiments. H.-h.Y., Y.-M.C., Y.-W.C., M.-Y.L, C.-C. L, and C.-C.C. analyzed the data. H.-h.Y. and C.-C.C. wrote the manuscript with feedback from all authors.

Source of founding

This work was supported by the Institute of Biomedical Sciences, Academia Sinica; the Taiwan Ministry of Science and Technology (MOST) (105-2320-B-001-020-MY3 and 108-2320-B-001-017-MY3) to C-CC.

Disclosures

None.

Declaration of competing interest

The authors declare that they have no known competing financial interests or personal relationships that could have appeared to influence the work reported in this paper.

Acknowledgments

We thank the Pathology Core and the Common Facilities Core Laboratory, the Proteomics Core Facility, and the Flow Cytometry core facility at the Institute of Biomedical Sciences (AS-CFII108-113), the Imaging Core Facility at the Institute of Cellular and Organismic Biology, and the High Throughput Sequencing Core at the Biodiversity Research Center (AS-CFII-108-114), Academia Sinica, Taiwan for their services and technical support.

Appendix A. Supplementary data

Supplementary data to this article can be found online at https://doi.org/10.1016/j.jmccpl.2022.100011.

References

[1] Fact sheets of cardiovascular diseases (CVDs). WHO/newsroom/fact sheets; 2021.
[2] Global status report on noncommunicable diseases 2014. WHO/Publications; 2014.
[3] Nakamura M, Sadoshima J. Mechanisms of physiological and pathological cardiac hypertrophy. Nat Rev Cardiol. 2018;15:387–407. https://doi.org/10.1038/s41569-018-0007-y.
[4] Grimm D, et al. Development of heart failure following isoproterenol administration in the rat: role of the renin-angiotensin system. Cardiovasc Res. 1998;37:91–100.
[5] Shiojima I, et al. Akt signaling mediates postnatal heart growth in response to insulin and nutritional status. J Biol Chem. 2002;277:37670–7. https://doi.org/10.1074/jbc.M204572200.
[6] McMullen JR, et al. The insulin-like growth factor 1 receptor induces physiological heart growth via the phosphoinositide 3-kinase(p110alpha) pathway. J Biol Chem. 2004;279:4782–93. https://doi.org/10.1074/jbc.M310405200.
[7] Palomeque J, Delbridge L, Petroff MV. Angiotensin II: a regulator of cardiomyocyte function and survival. Front Biosci. 2009;14:5118–33.
[8] Maillet M, van Berlo JH, Molkentin JD. Molecular basis of physiological heart growth: fundamental concepts and new players. Nat Rev Mol Cell Biol. 2013;14:38–48. https://doi.org/10.1038/nrm3495.
[9] van Berlo JH, Maillet M, Molkentin JD. Signaling effectors underlying pathologic growth and remodeling of the heart. J Clin Invest. 2013;123:37–45. https://doi.org/10.1172/JCI62839.
[10] Westphal JG, Bekfani T, Schulze PC. What's new in heart failure therapy 2018? Interact Cardiovasc Thorac Surg. 2018;27:921–30. https://doi.org/10.1093/icvts/ivy282.
[11] Pellicori P, Khan MJI, Graham FJ, Cleland JGF. New perspectives and future directions in the treatment of heart failure. Heart Fail Rev. 2020;25:147–59. https://doi.org/10.1007/s10741-019-09829-7.
[12] Schiaffino S, et al. Nonsynchronous accumulation of alpha-skeletal actin and beta-myosin heavy chain mRNAs during early stages of pressure-overload–induced cardiac hypertrophy demonstrated by in situ hybridization. Circ Res. 1989;64:937–48.
[13] Prestle J, Dieterich S, Preuss M, Bieligk U, Hasenfuss G. Heterogeneous transmural gene expression of calcium-handling proteins and natriuretic peptides in the failing human heart. Cardiovasc Res. 1999;43:323–31.
[14] Pandya K, Kim HS, Smithies O. Fibrosis, not cell size, delineates beta-myosin heavy chain reexpression during cardiac hypertrophy and normal aging in vivo. Proc Natl Acad Sci U S A. 2006;103:16864–9. https://doi.org/10.1073/pnas.0607700103.
[15] Lopez JE, et al. Beta-myosin heavy chain is induced by pressure overload in a minor subpopulation of smaller mouse cardiac myocytes. Circ Res. 2011;109:629–38. https://doi.org/10.1161/CIRCRESAHA.111.243410.
[16] Li G, et al. Transcriptomic profiling maps anatomically patterned subpopulations among single embryonic cardiac cells. Dev Cell. 2016;39:491–507. https://doi.org/10.1016/j.devcel.2016.10.014.
[17] DeLaughter DM, et al. Single-cell resolution of temporal gene expression during heart development. Dev Cell. 2016;39:480–90. https://doi.org/10.1016/j.devcel.2016.10.001.
[18] Liu Z, et al. Single-cell transcriptomics reconstructs fate conversion from fibroblast to cardiomyocyte. Nature. 2017;551:100–4. https://doi.org/10.1038/nature24454.
[19] Nomura S, et al. Cardiomyocyte gene programs encoding morphological and functional signatures in cardiac hypertrophy and failure. Nat Commun. 2018;9:4435. https://doi.org/10.1038/s41467-018-06639-7.
[20] Ren Z, et al. Single-cell reconstruction of progression trajectory reveals intervention principles in pathological cardiac hypertrophy. Circulation. 2020. https://doi.org/10.1161/CIRCULATIONAHA.119.043053.
[21] Hu P, et al. Minimally invasive aortic banding in mice: effects of altered cardiomyocyte insulin signaling during pressure overload. Am J Physiol Heart Circ Physiol. 2003;285:H1261–9. https://doi.org/10.1152/ajpheart.00108.2003.
[22] Kolwicz Jr SC, et al. Cardiac-specific deletion of acetyl CoA carboxylase 2 prevents metabolic remodeling during pressure-overload hypertrophy. Circ Res. 2012;111:728–38. https://doi.org/10.1161/CIRCRESAHA.112.268128.
[23] Bertero E, Maack C. Metabolic remodelling in heart failure. Nat Rev Cardiol. 2018;15:457–70. https://doi.org/10.1038/s41569-018-0044-6.
[24] Gibb AA, Hill BG. Metabolic coordination of physiological and pathological cardiac remodeling. Circ Res. 2018;123:107–28. https://doi.org/10.1161/CIRCRESAHA.118.312017.
[25] Karwi QG, Uddin GM, Ho KL, Lopaschuk GD. Loss of metabolic flexibility in the failing heart. Front Cardiovasc Med. 2018;5:68. https://doi.org/10.3389/fcvm.2018.00068.
[26] Xu M, et al. Choline ameliorates cardiac hypertrophy by regulating metabolic remodelling and UPRmt through SIRT3-AMPK pathway. Cardiovasc Res. 2018. https://doi.org/10.1093/cvr/cvy217.
[27] Tran DH, Wang ZV. Glucose metabolism in cardiac hypertrophy and heart failure. J Am Heart Assoc. 2019;8:e012673. https://doi.org/10.1161/JAHA.119.012673.
[28] Stahl PL, et al. Visualization and analysis of gene expression in tissue sections by spatial transcriptomics. Science. 2016;353:78–82. https://doi.org/10.1126/science.aaf2403.
[29] Lein E, Borm LE, Linnarsson S. The promise of spatial transcriptomics for neuroscience in the era of molecular cell typing. Science. 2017;358:64–9. https://doi.org/10.1126/science.aan6827.
[30] Moor AE, Itzkovitz S. Spatial transcriptomics: paving the way for tissue-level systems biology. Curr Opin Biotechnol. 2017;46:126–33. https://doi.org/10.1016/j.copbio.2017.02.004.
[31] Burgess DJ. Transcriptomics: finding structure in gene expression. Nat Rev Genet. 2018;19:249. https://doi.org/10.1038/nrg.2018.19.
[32] Maniatis S, et al. Spatiotemporal dynamics of molecular pathology in amyotrophic lateral sclerosis. Science. 2019;364. https://doi.org/10.1126/science.aav9776. 89-+.
[33] Chiang CS, et al. The Ca(v)3.2 T-type Ca2+ channel is required for pressure overload-induced cardiac hypertrophy in mice. Circ Res. 2009;104. https://doi.org/10.1161/Circresaha.108.184051. 522-U194.
[34] Satija R, Farrell JA, Gennert D, Schier AF, Regev A. Spatial reconstruction of single-cell gene expression data. Nat Biotechnol. 2015;33:495–502. https://doi.org/10.1038/nbt.3192.
[35] Butler A, Hoffman P, Smibert P, Papalexi E, Satija R. Integrating single-cell transcriptomic data across different conditions, technologies, and species. Nat Biotechnol. 2018;36:411–20. https://doi.org/10.1038/nbt.4096.
[36] Stuart T. Comprehensive integration of single-cell data. Cell. 2019;177:1888–902. https://doi.org/10.1016/j.cell.2019.05.031. e1821.
[37] Wolf FA, Angerer P, Theis FJ. SCANPY: large-scale single-cell gene expression data analysis. Genome Biol. 2018;19:15. https://doi.org/10.1186/s13059-017-1382-0.
[38] Skrzypiec-Spring M, Grotthus B, Szelag A, Schulz R. Isolated heart perfusion according to Langendorff—still viable in the new millennium. J Pharmacol Toxicol Methods. 2007;55:113–26. https://doi.org/10.1016/j.vascn.2006.05.006.
[39] O'Connell TD, Rodrigo MC, Simpson PC. Isolation and culture of adult mouse cardiac myocytes. Methods Mol Biol. 2007;357:271–96. https://doi.org/10.1385/1-59745-214-9:271.
[40] Trapnell C, Pachter L, Salzberg SL. TopHat: discovering splice junctions with RNA-seq. Bioinformatics. 2009;25:1105–11. https://doi.org/10.1093/bioinformatics/btp120.
[41] Langmead B, Trapnell C, Pop M, Salzberg SL. Ultrafast and memory-efficient alignment of short DNA sequences to the human genome. Genome Biol. 2009;10:R25. https://doi.org/10.1186/gb-2009-10-3-r25.
[42] Trapnell C, et al. Transcript assembly and quantification by RNA-seq reveals unannotated transcripts and isoform switching during cell differentiation. Nat Biotechnol. 2010;28:511–5. https://doi.org/10.1038/nbt.1621.
[43] Tarazona S, et al. Data quality aware analysis of differential expression in RNA-seq with NOISeq R/Bioc package. Nucleic Acids Res. 2015;43:e140. https://doi.org/10.1093/nar/gkv711.
[44] Parker BL, et al. Multiplexed temporal quantification of the exercise-regulated plasma peptidome. Mol Cell Proteomics. 2017;16:2055–68. https://doi.org/10.1074/mcp.RA117.000020.
[45] Kramer A, Green J, Pollard Jr J, Tugendreich S. Causal analysis approaches in ingenuity pathway analysis. Bioinformatics. 2014;30:523–30. https://doi.org/10.1093/bioinformatics/btt703.
[46] Zhou Y, et al. Metascape provides a biologist-oriented resource for the analysis of systems-level datasets. Nat Commun. 2019;10:1523. https://doi.org/10.1038/s41467-019-09234-6.
[47] Subramanian A, et al. Gene set enrichment analysis: a knowledge-based approach for interpreting genome-wide expression profiles. Proc Natl Acad Sci U S A. 2005;102:15545–50. https://doi.org/10.1073/pnas.0506580102.
[48] Mootha VK, et al. PGC-1alpha-responsive genes involved in oxidative phosphorylation are coordinately downregulated in human diabetes. Nat Genet. 2003;34:267–73. https://doi.org/10.1038/ng1180.
[49] Perez-Riverol Y, et al. The PRIDE database and related tools and resources in 2019: improving support for quantification data. Nucleic Acids Res. 2019;47:D442–50. https://doi.org/10.1093/nar/gky1106.
[50] Odiete O, Hill MF, Sawyer DB. Neuregulin in cardiovascular development and disease. Circ Res. 2012;111:1376–85. https://doi.org/10.1161/Circresaha.112.267286.
[51] O'Neal WT, et al. Ephrin-eph signaling as a potential therapeutic target for the treatment of myocardial infarction. Med Hypotheses. 2013;80:738–44. https://doi.org/10.1016/j.mehy.2013.02.024.
[52] Galindo CL, Ryzhov S, Sawyer DB. Neuregulin as a heart failure therapy and mediator of reverse remodeling. Curr Heart Fail Rep. 2014;11:40–9. https://doi.org/10.1007/s11897-013-0176-2.
[53] Su SA, et al. EphrinB2 regulates cardiac fibrosis through modulating the interaction of Stat3 and TGF-beta/Smad3 signaling. Circ Res. 2017;121. https://doi.org/10.1161/Circresaha.117.311045. 617-+.
[54] Santos-Ribeiro D, Godinas L, Pilette C, Perros F. The integrated stress response system in cardiovascular disease. Drug Discov Today. 2018;23:920–9. https://doi.org/10.1016/j.drudis.2018.02.008.
[55] Hu YX, et al. Epitranscriptional orchestration of genetic reprogramming is an emergent property of stress-regulated cardiac microRNAs. Proc Natl Acad Sci U S A. 2012;109:19864–9. https://doi.org/10.1073/pnas.1214996109.
[56] Long PA, Larsen BT, Evans JM, Olson TM. Exome sequencing identifies pathogenic and. J Am Heart Assoc. 2015;4:e002443. https://doi.org/10.1161/JAHA.115.002443.

[57] Farrell E, et al. Transcriptome analysis of cardiac hypertrophic growth in MYBPC3-null mice suggests early responders in hypertrophic remodeling. Front Physiol. 2018;9:1442. https://doi.org/10.3389/fphys.2018.01442.
[58] Harston RK, Kuppuswamy D. Integrins are the necessary links to hypertrophic growth in cardiomyocytes. J Signal Transduct. 2011;2011:521742. https://doi.org/10.1155/2011/521742.
[59] Chen C, Li R, Ross RS, Manso AM. Integrins and integrin-related proteins in cardiac fibrosis. J Mol Cell Cardiol. 2016;93:162–74. https://doi.org/10.1016/j.yjmcc.2015.11.010.
[60] Tsika RW, et al. TEAD-1 overexpression in the mouse heart promotes an age-dependent heart dysfunction. J Biol Chem. 2010;285:13721–35. https://doi.org/10.1074/jbc.M109.063057.
[61] Rose BA, Force T, Wang Y. Mitogen-activated protein kinase signaling in the heart: angels versus demons in a heart-breaking tale. Physiol Rev. 2010;90:1507–46. https://doi.org/10.1152/physrev.00054.2009.
[62] Dixon IMC, Hao JM, Reid NL, Roth JC. Effect of chronic AT(1) receptor blockade on cardiac smad overexpression in hereditary cardiomyopathic hamsters. Cardiovasc Res. 2000;46:286–97. https://doi.org/10.1016/S0008-6363(00)00035-3.
[63] Schneiders D, Heger J, Best P, Michael Piper H, Taimor G. SMAD proteins are involved in apoptosis induction in ventricular cardiomyocytes. Cardiovasc Res. 2005;67:87–96. https://doi.org/10.1016/j.cardiores.2005.02.021.
[64] Bjornstad JL, et al. Inhibition of SMAD2 phosphorylation preserves cardiac function during pressure overload. Cardiovasc Res. 2012;93:100–10. https://doi.org/10.1093/cvr/cvr294.
[65] Chiaravalli M, et al. 2-deoxy-d-glucose ameliorates PKD progression. J Am Soc Nephrol. 2016;27:1958–69. https://doi.org/10.1681/ASN.2015030231.
[66] Enzo E, et al. Aerobic glycolysis tunes YAP/TAZ transcriptional activity. EMBO J. 2015;34:1349–70. https://doi.org/10.15252/embj.201490379.
[67] Tran DH, et al. Chronic activation of hexosamine biosynthesis in the heart triggers pathological cardiac remodeling. Nat Commun. 2020;11:1771. https://doi.org/10.1038/s41467-020-15640-y.
[68] Pandya K, Porter K, Rockman HA, Smithies O. Decreased beta-adrenergic responsiveness following hypertrophy occurs only in cardiomyocytes that also re-express beta-myosin heavy chain. Eur J Heart Fail. 2009;11:648–52. https://doi.org/10.1093/eurjhf/hfp073.
[69] Kockskamper J, Zima AV, Blatter LA. Modulation of sarcoplasmic reticulum Ca2+ release by glycolysis in cat atrial myocytes. J Physiol. 2005;564:697–714. https://doi.org/10.1113/jphysiol.2004.078782.
[70] Dejos C, Gkika D, Cantelmo AR. The two-way relationship between calcium and metabolism in cancer. Front Cell Dev Biol. 2020;8:573747. https://doi.org/10.3389/fcell.2020.573747.
[71] Etchegaray JP, Mostoslavsky R. Interplay between metabolism and epigenetics: a nuclear adaptation to environmental changes. Mol Cell. 2016;62:695–711. https://doi.org/10.1016/j.molcel.2016.05.029.
[72] Angrisano T, et al. Epigenetic switch at Atp2a2 and Myh7 gene promoters in pressure overload-induced heart failure. PloS one. 2014;9:e106024. https://doi.org/10.1371/journal.pone.0106024.